mater.scichina.com link.springer.com

Published online 10 February 2021 | https://doi.org/10.1007/s40843-020-1575-2
Sci China Mater 2021, 64(7): 1742–1750

Highly structured metal-organic framework nanofibers for methane storage

Yibo Dou[1,2], Carlos Grande[3], Andreas Kaiser[1*] and Wenjing Zhang[2*]

ABSTRACT **Porous materials such as metal-organic frameworks (MOFs) with high theoretical volumetric gas uptake capacity are promising materials for gas storage and separation, but the structuring for practical applications is challenging. Herein, we report a general and feasible strategy to combine electrospinning with a phase conversion method to decorate polyacrylonitrile nanofibers (PAN NFs) with Cu-MOF (HKUST-1). The strategy is based on the combination of surface pretreatment of the NFs with $Cu(OH)_2$ and a subsequent phase conversion into HKUST-1 crystals (PC-HKUST-1). A significant higher loading of HKUST-1 in the PAN NF matrix was achieved by the phase conversion method compared with direct electrospinning of MOF slurries or *in-situ* growth of MOF crystals on NFs. As a result, the hierarchical structured PC (phase conversion)-HKUST-1 NFs revealed the highest gravimetric storage capacity of 86 cm^3 g^{-1} (STP) at 3500 kPa and 298 K for methane (CH_4), which is higher than other HKUST-1 NFs reported previously. The improved CH_4 uptake can be explained by the high loading of HKUST-1 due to the high availability of Cu-ions localized on the surface of the NFs during the phase conversion process, resulting in high surface area and excellent gas access of the phase converted HKUST-1. Thus, the developed strategy of structuring MOFs could be of interest for the fabrication of tailor-made MOF NF architectures for other energy and environmental applications.**

Keywords: electrospinning, phase conversion, metal-organic frameworks (MOFs), methane storage

INTRODUCTION

Growing concerns on the increasing consumption and combustion of fossil fuels and related environmental issues have stimulated the development of renewable energy [1–3]. Methane (CH_4) is considered as a preferable alternative energy source, owing to its increasing supply and low emission of greenhouse gases with the option to produce sustainable fuel from biogas [4–6]. However, the low volumetric energy density of 0.038 MJ L^{-1}, as compared with liquid fuels (such as gasoline, with a volumetric energy density of 34.8 MJ L^{-1}), limits the practical application, especially in vehicular transportation [7,8]. Therefore, the concept of compressed natural gas (CNG) is widely applied, where CH_4 is compressed at approximately 20 MPa to increase the volumetric storage capacity. For automotive vehicles, storing CH_4 on board at such high pressure requires multiple stages of compression (hence increases the costs) and presents safety restrictions [9]. Adsorbed natural gas (ANG) allows storing CH_4 on porous materials and can result in high volumetric storage density at a much lower pressure with a single compression stage [10–13]. In the ANG system, the adsorption capacity and the structure of the porous material play a vital role for the adsorption/desorption processes. Metal-organic frameworks (MOFs) are regarded as promising porous materials due to their high surface area, high porosity, tunable pore size and rich chemistry properties [14–18]. Previous research work demonstrated record-breaking gas-storage capacities of MOFs in laboratory environment. However, from a practical application point of view, the MOFs need to be structured into macroscopic shapes to ensure structural robustness and integrity in the ANG system. Traditional powder shaping methods, such as extrusion and granulation, utilize high pressure or chemical binders to form wafers or pellets [19]. These structuring processes often inevitably deteriorate the intrinsic properties of single-crystal MOFs, leading to low crystallographic density and

[1] Department of Energy Conversion and Storage, Technical University of Denmark, Anker Angelundsvej, DK-2800 Kongens Lyngby, Denmark
[2] Department of Environmental Engineering, Technical University of Denmark, Miljøvej 113, DK-2800 Kongens Lyngby, Denmark
[3] SINTEF, SINTEF AS. Forskningsveien 1. 0373 Oslo, Norway
* Corresponding authors (emails: akai@dtu.dk (Kaiser A); wenz@dtu.dk (Zhang W))

collapsed porosity and hence decreased gas storage capacity [19]. Therefore, to advance practical applications of MOFs in ANG technology, it is an essential step to develop novel methods that can structure MOFs into suitable macroscopic shapes without sacrificing their excellent gas storage properties.

Recently, the structuring of MOFs with various techniques, including dip-coating, spray-drying, three-dimensional (3D)-printing and lithography, have attracted considerable attention [20–22]. We recently summarized advances in the synthesis and structuring of MOFs/polymer nanofibers (NFs) [23], which have been widely investigated for energy and environmental applications [24–28]. Up to now, the most prevailing method is direct electrospinning (DE) of a mixture of MOFs and polymers [29–31]. However, the coverage of the surface of MOFs by polymers would inevitably lead to severe blockage of the inner pores of the MOFs and hinder the mass transfer and adsorption of gas molecules. Alternately, an *in-situ* growth (IG) method was proposed to anchor MOFs on the polymer NF surface [32–34]. Despite the highly exposed pores, the low mass fraction of MOFs in the resulting MOFs/polymer NF composites still limits the overall gas adsorption capacity.

Phase conversion is a recently developed method for the synthesis of MOFs by converting a dense, crystalline phase of a metal oxide as the precursor to a less dense, crystalline MOF product phase [14,24]. In this work, we developed a novel way to conduct the phase conversion directly on electrospun NF structures, which resulted in MOF NF composite mats with the MOF nanocrystals exposed on the surface of the NFs. Unlike conventional methods for structuring MOFs, the new method enables high MOF loading in the NF scaffold with a combination of fascinating properties towards efficient CH_4 storage, including excellent structural integrity, flexibility and accessibility of CH_4 gas molecules to the porosities of MOF crystals. As a result, the MOF NF mat prepared by the phase conversion method offers a superior CH_4 uptake capacity as compared with the MOF NFs prepared by DE and IG methods.

EXPERIMENTAL SECTION

Fabrication of PAN NFs

The polyacrylonitrile NFs (PAN NFs) were prepared by the electrospinning method. Typically, 10 g of PAN was dissolved in 90 g of *N*,*N*-dimethylformamide (DMF) under ball milling for 72 h. The PAN NFs were obtained by electrospinning at a flow rate of 1 mL h^{-1} in a syringe (10 mL). A high voltage of 35 kV was used, and the distance between the collector and spinneret was set at 12 cm.

Fabrication of PAN/$Cu(OH)_2$ NFs

Prior to fabrication, the above PAN mat was peeled off from the substrate and immersed in water for 10 min to wet the PAN mat surface. The overall synthesis procedure consists of a cyclic repetition *via* the following steps: (1) immersing the PAN mat into an aqueous solution of NaOH (8 wt%) for 3 min, followed by rinsing with deionized water thoroughly; (2) immersing the PAN mat into an aqueous solution of $Cu(NO_3)_2{\cdot}3H_2O$ (24 wt%) for 3 min followed by washing with deionized water. Subsequently, the PAN/$Cu(OH)_2$ fibrous mats were fabricated by an alternating deposition of NaOH and $Cu(NO_3)_2{\cdot}3H_2O$ solution for four cycles. The PAN/$Cu(OH)_2$ fibrous mats were finally rinsed with deionized water and dried at room temperature (RT).

Fabrication of PC-HKUST-1 NFs

The PAN NFs with Cu-MOF (HKUST-1) were fabricated *via* the phase conversion method (Method 3 in Fig. 1). For this purpose, 3 g of 1,3,5-benzenetricarboxylic acid was dissolved into 160 mL of methanol, and then the PAN/$Cu(OH)_2$ NFs were immersed into the above solution. After reacting for 24 h at RT, the PAN/$Cu(OH)_2$ NFs were converted into the PC (phase conversion)-HKUST-1 NFs. The obtained PC-HKUST-1 NFs were finally rinsed with ethanol and dried at RT. The loading of HKUST-1 by weight in the PC-HKUST-1 NFs is ~52 wt%.

Fabrication of IG-HKUST-1 NFs

The IG-HKUST-1 NFs (Method 2 in Fig. 1) were fabricated by the IG method. First, PAN@$Cu(OH)_2$ NFs were prepared by electrospinning. First, 10 g of PAN and 5 g of $Cu(OH)_2$ were dissolved in 90 g of DMF under ball milling for 72 h. The PAN@$Cu(OH)_2$ NFs were fabricated by electrospinning at a flow rate of 0.8 mL h^{-1} in a syringe (10 mL). A high voltage of 35 kV was used, and the distance between the collector and spinneret was set at 12 cm. Then, 5 g of 1,3,5-benzenetricarboxylic acid was dissolved into 160 mL of methanol, and the PAN@$Cu(OH)_2$ NFs were immersed into the above solution. After reacting for 24 h at RT, the PAN@$Cu(OH)_2$ NFs were converted into IG-HKUST-1 NFs. The obtained IG-HKUST-1 NFs were finally rinsed with ethanol and dried at RT. The loading of HKUST-1 by weight in IG-HKUST-1 NFs is only ~28 wt%.

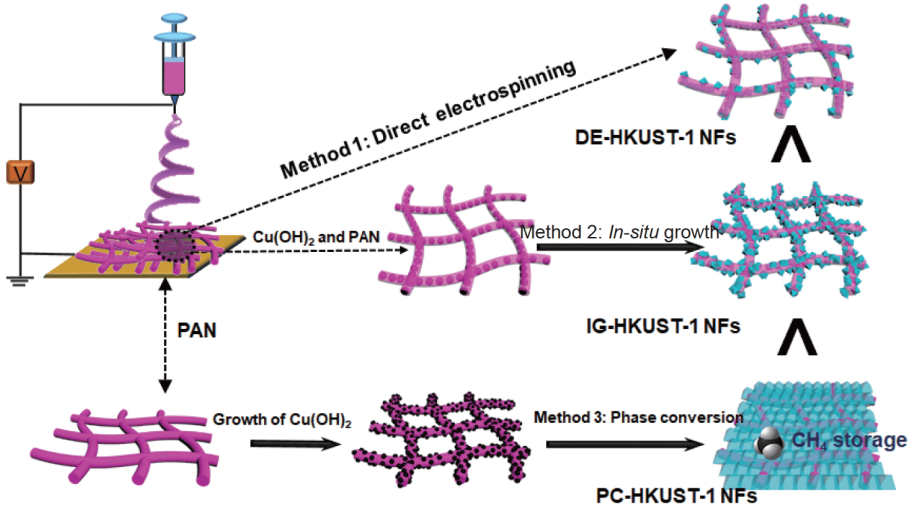

Figure 1 Illustration of different synthesis routes for structuring HKUST-1 into MOF NFs. Method 1: DE-HKUST-1 NFs fabricated by directly electrospinning a slurry of HKUST-1 and PAN; Method 2: IG-HKUST-1 NFs fabricated by *in-situ* growth of HKUST-1 on the surface of NFs; Method 3: PC-HKUST-1 NFs fabricated by our new method where HKUST-1 layer is combined with the NFs.

Fabrication of DE-HKUST-1 NFs

The DE-HKUST-1 NFs were fabricated by the DE method (Method 1 in Fig. 1). The HKUST-1 powder was prepared following a previously reported method [34]. Then, 7.5 g of PAN and 2.5 g of HKUST-1 were dissolved in 90 g of DMF under ball milling for 72 h. The DE-HKUST-1 NFs were electrospun at a flow rate of 0.8 mL h^{-1} in a syringe (10 mL). A high voltage of 35 kV was used, and the distance between the collector and spinneret was set at 12 cm. The loading of HKUST-1 by weight in DE-HKUST-1 NF is ~25 wt%.

Fabrication of HKUST-1 powder

Traditional HKUST-1 powder was synthesized according to a previously reported method [35,36]. As for phase converted HKUST-1 powder, the above obtained 0.5 g $Cu(OH)_2$ was added into 1,3,5-benzenetricarboxylic acid (0.8 g) that dissolved in 40 mL methanol under stirring for 5 min. Then the solution was incubated without stirring at RT for 24 h. The obtained solid was collected by centrifugation, washed with ethanol and dried in vacuum at RT.

Characterization

Powder X-ray diffraction (PXRD) patterns of HKUST-1 and $Cu(OH)_2$ were recorded in a Rigaku XRD-6000 diffractometer (Japan) with Cu Kα radiation (λ = 0.1542 nm) at 40 kV and 30 mA. X-ray photoelectron spectroscopy (XPS) measurements were performed in an ESCALAB 250 instrument (Thermo Electron, USA) with Al Kα radiation to investigate the interaction between HKUST-1 and PAN. The morphology of the NFs was observed using a scanning electron microscope (SEM; Zeiss 1540XB, Germany) with an accelerating voltage of 5–15 kV, combined with energy-dispersive X-ray spectroscopy (EDX) for the determination of composition. The specific surface area determination and pore size analysis were performed by Brunauer-Emmett-Teller (BET) methods, respectively, using a Quantachrome autosorb analyzer (USA). Prior to the measurements, the samples were degassed at 120°C for 6 h. Fourier-transform infrared (FTIR) spectroscopy was obtained using a Vector 22 (Bruker) spectrophotometer (Germany). The measurements of CH_4 excess adsorption on different materials were evaluated in a Belsorp HP unit using CH_4 with purity higher than 99.995% without any further treatment. All samples were degassed at 120°C for 10 h under vacuum. In addition, the CH_4 isotherm fitting parameters for multi-site Langmuir isotherm equation were provided as well, the specific fitting process can be found in our previous work [37].

RESULTS AND DISCUSSION

Synthesis and structuring of MOFs

In order to determine the performance of MOF NFs for gas storage, HKUST-1 NFs were prepared by three different methods as described in Fig. 1: Method 1, DE of a slurry mixture of PAN and HKUST-1 to obtain DE-HKUST-1 NFs; Method 2, *in-situ* growth of HKUST-1 on

the surface of PAN@$Cu(OH)_2$ NFs, resulting in IG-HKUST-1 NFs; Method 3, a combination of electrospinning with phase conversion is proposed to obtain PC-HKUST-1 NFs. It is obvious that these three types of MOF NFs display quite different morphologies. The SEM image of DE-HKUST-1 NFs (Fig. 2a) shows HKUST-1 nanoparticles, which are encapsulated by the PAN matrix. The HKUST-1 loading of the sample was determined to be ~25 wt%. On the contrary, the SEM image of IG-HKUST-1 NFs in Fig. 2b shows HKUST-1 nanoparticles that are anchored on the surface of PAN NFs, which is favorable for exposure of the pores of MOF particles for gas adsorption. It should be noted that the loading of HKUST-1 is only ~28 wt% in this case. As a result, there is still a large void fraction in the fibrous mat, which would limit the gas storage capacity of the composite MOFs. In contrast, Method 3 promotes the growth of HKUST-1 crystals not only on the surface of the NFs but also within the void space of the porous NF structure (Fig. 2e). The propagation of the growth of the HKUST-1 crystals has resulted in a loading of HKUST-1 of ~52 wt% in PC-HKUST-1 NFs. This is an exceptional improvement in the HKUST-1 loading compared with Methods 1 and 2. The significantly improved MOF loading achieved by this method opens several opportunities to improve the gas storage capacity of MOF NF composite in different gas separation and storage applications.

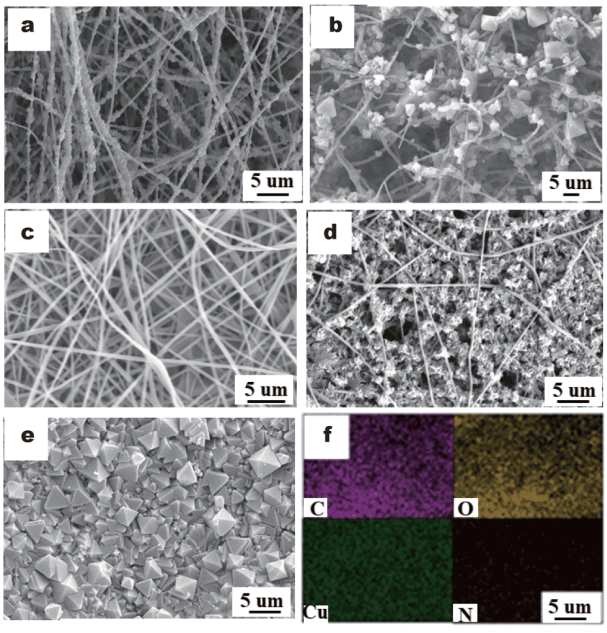

Figure 2 SEM images for (a) DE-HKUST-1 NFs, (b) IG-HKUST-1 NFs, (c) pure PAN NFs, (d) PAN/$Cu(OH)_2$ NFs and (e) PC-HKUST-1 NFs with (f) corresponding EDX mapping.

Since PC-HKUST-1 NFs exhibited significantly higher HKUST-1 loading than the other samples, we carried out further systematic studies of the phase conversion method and the resulting material, including microstructural and compositional characterizations as well as CH_4 adsorption tests. The morphologies of the PC-HKUST-1 NFs after each fabrication step are shown in Fig. 2 with the PAN NFs after electrospinning (Fig. 2c), the PAN/$Cu(OH)_2$ after the formation of $Cu(OH)_2$ in the macropores of the PAN NFs (Fig. 2d), and the PC-HKUST-1 NFs after the phase conversion of $Cu(OH)_2$ into HKUST-1 (Fig. 2e). In Fig. 2c, the electrospun PAN NFs have an average diameter of 450 nm. These PAN NFs were immersed subsequently in a $Na(OH)_2$ solution and a $Cu(NO_3)_2$ solution to achieve the growth of $Cu(OH)_2$ crystals on the PAN NFs. It should be noted that the alkaline solution was used to activate the PAN surface by forming the hydroxide groups. The hydroxide groups can react with Cu^{2+} for the formation of $Cu(OH)_2$ particles on the surface of PAN NFs. Finally, the phase conversion was initiated by immersing the resulting NFs mat in the 1,3,5-benzenetricarboxylic acid solution, which transformed the PAN/$Cu(OH)_2$ NFs to the PC-HKUST-1 NFs mats with light blue color (Fig. S1). As shown in Fig. 2e, the void space in the pristine porous NF structure seems to be fully occupied by HKUST-1 crystals. The dense composite NF mat is composed of ~52 wt% HKUST-1 crystals for CH_4 adsorption and ~48 wt% PAN NFs for improved structural stability and flexibility. In addition, the uniform distribution of O, C, Cu and N elements on PC-HKUST-1 NFs was confirmed by EDX analysis (Fig. 2f). Furthermore, we successfully synthesized two other types of PC-MOFs NFs, by the phase conversion method from PAN/$Zn(OH)_2$ and PAN/$Co(OH)_2$ NFs in 2-methylimidazole solution, resulting in ZIF-8 NFs and ZIF-67 NFs, respectively (Figs S2 and S3). Similarly, the surfaces of the PAN NFs are fully covered by the MOF crystals in both cases. Therefore, we believe that the proposed phase conversion method can be more widely applied for the structuring of various MOF NFs.

Structural characterization

The composition and crystal structure of PC-HKUST-1 NFs were studied by XRD and FTIR spectroscopy. Fig. 3a shows the XRD patterns of the PAN/$Cu(OH)_2$ NFs. A series of reflection peaks of PAN/$Cu(OH)_2$ matched well with $Cu(OH)_2$ (JCPDS NO. 13-420). After the phase conversion, a series of new diffraction peaks at 2θ of 6.61°, 9.33°, 11.35°, 14.55°, 16.78°, and 18.92° were observed, which are corresponding to the (200), (220),

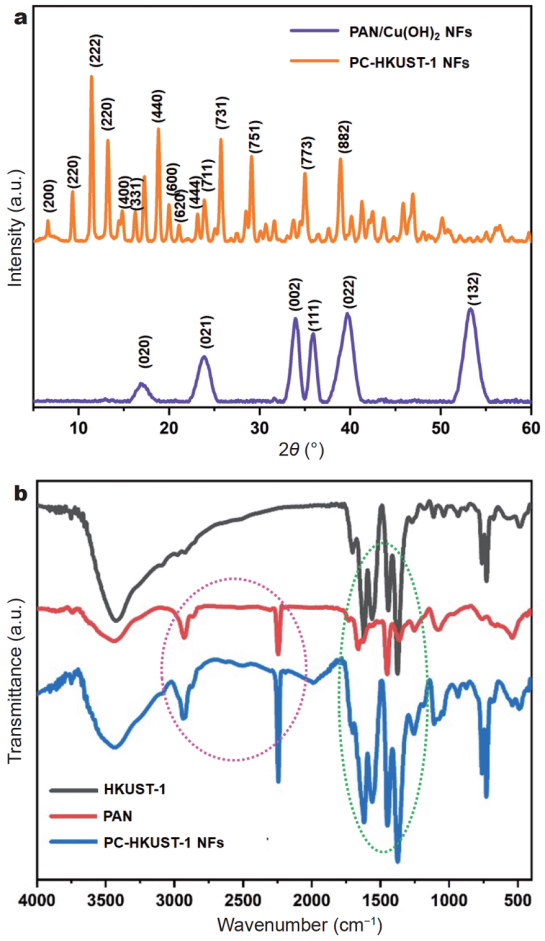

Figure 3 (a) Powder XRD patterns of PAN/$Cu(OH)_2$ and PC-HKUST-1 NFs, respectively. (b) FTIR spectra of PAN, HKUST-1 and PC-HKUST-1 NFs, respectively.

(222), (400), (331), and (440) reflections of HKUST-1 for PC-HKUST-1 NFs. No other new diffraction peaks were observed in the XRD pattern of HKUST-1, indicating the $Cu(OH)_2$ is efficiently converted into HKUST-1. Moreover, the FTIR spectra also confirmed the existence of both HKUST-1 and PAN in the composite structure (Fig. 3b). For the PC-HKUST-1 NFs, characteristic absorption peaks of the –COO group from HKUST-1 were observed at 1645, 1620, 1570, and 1550 cm^{-1}. Meanwhile, the stretching vibrations of the C≡N centered at 2247 cm^{-1} and the –CH and $–CH_2$ groups centered at 2927 cm^{-1} were observed, which can be attributed to the PAN scaffold in the PC-HKUST-1 NFs. The FTIR spectra and XRD patterns demonstrate that crystalline HKUST-1 with high purity can be grown by phase conversion into a PAN NF matrix.

In order to understand the interaction between the HKUST-1 and PAN in PC-HKUST-1 NFs, fine-scan XPS measurements were carried out. As shown in Fig. 4a, in the case of pure PAN NFs, the binding energy of N 1s is centered at 400.1 eV. After the growth of the HKUST-1 on the PAN NFs by the phase conversion method, a shift of 0.9 eV in the binding energy was observed. Moreover, the binding energies of Cu 2p of PC-HKUST-1 NFs exhibited a positive shift as compared with that of pristine HKUST-1 nanoparticles (Fig. 4b). The shifts in the binding energies of Cu 2p and N 1s indicate the existence of mild interaction between HKUST-1 and PAN. It is our hypothesis that this interaction contributes to the excellent adhesion of HKUST-1 crystals on the PAN NFs scaffolds. It should be noted that this excellent adhesion offers structural integrity of hierarchical structured PC-HKUST-1 NF mat, which would be favorable for sustaining the high pressure and temperature swings during the gas adsorption/desorption processes.

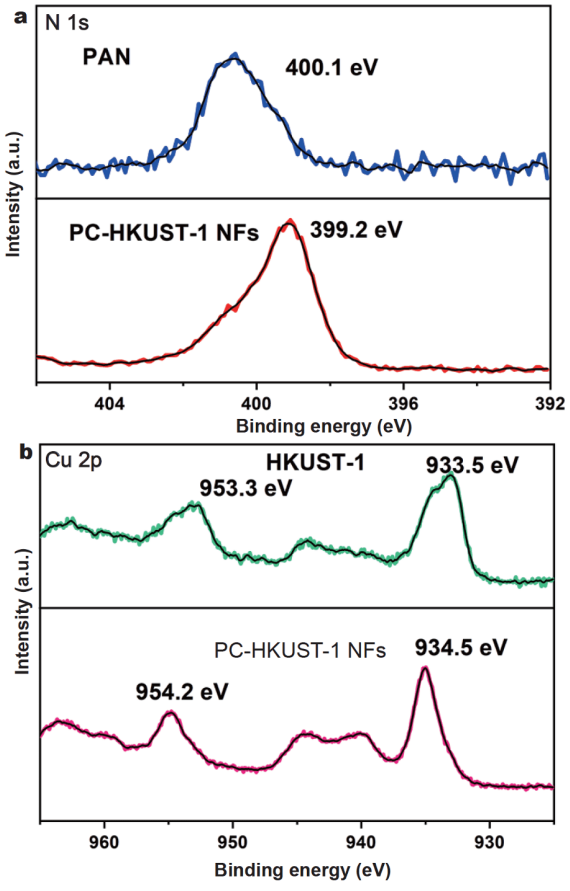

Figure 4 XPS spectra of (a) N 1s of PAN NFs and PC-HKUST-1 NFs, (b) Cu 2p of HKUST-1 powder and PC-HKUST-1 NFs, respectively.

Evaluation of CH_4 uptake capability

A very high surface area of the structured MOFs is important for CH_4 storage. We carried out surface area measurements on all NF samples by N_2 adsorption/desorption measurements (Fig. 5a). Pure PAN NFs show a surface area of ~19 $m^2 g^{-1}$ (Fig. S4). After the incorporation of $Cu(OH)_2$ into the PAN mats, an increase in surface area to ~120 $m^2 g^{-1}$ was observed (Fig. S5). By phase conversion, the $Cu(OH)_2$ particles were converted into microporous HKUST-1 crystals. As a consequence, the surface area of the resulting PC-HKUST-1 NF mat increases from ~120 to ~765 $m^2 g^{-1}$. For comparison, we also synthesized HKUST-1 powder by a previously reported method [36], and the BET results show a surface area of ~1190 $m^2 g^{-1}$ (Figs S6 and S7). The lower surface area of PC-HKUST-1 NFs compared with pure HKUST-1 powder can be explained by the presence of 48 wt% PAN NFs as scaffold material, which has a much lower surface area (~19 $m^2 g^{-1}$). Moreover, in all cases of MOF NFs, typical IV isotherms with H3-type hysteresis loops (P/P_0 > 0.4) are observed, indicating the presence of mesopores in all three samples. Interestingly, no obvious hysteresis loops are found for the HKUST-1 powder. Compared with other MOF NFs, PC-HKUST-1 NFs exhibit larger hysteresis loops, indicating the formation of slit-shaped pores formed by the stacking of HKUST-1 layer on PAN NFs. In addition, the pore size distribution indicated that the PC-HKUST-1 NFs displayed a hierarchical pore structure (Fig. S8), which is generated by the fibrous structure and the intrinsic MOF structure. Such a hierarchical pore structure is favorable for gas transport and for exposing the active MOF sites for the adsorption of CH_4. Subsequently, the CH_4 isothermal adsorption curves for all the samples were studied. As shown in Fig. 5b, the CH_4 uptake volumes of DE-HKUST-1 NFs, IG-HKUST-1 NFs and PC-HKUST-1 NFs are 2.5, 6.2 and 18.1 $cm^3 g^{-1}$, respectively. We thus conclude that largely improved surface area and gas adsorption capacities can be achieved by the structuring of MOFs in composite mats if the phase conversion method is used.

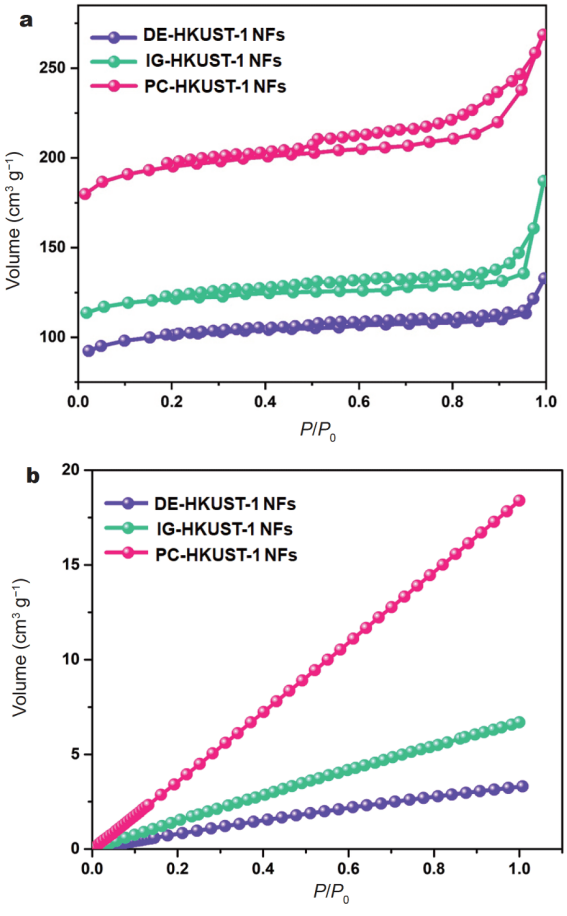

Figure 5 (a) N_2 adsorption/desorption curves and (b) CH_4 isothermal adsorption curves at 298 K for different NF mats: DE-HKUST-1 NFs, IG-HKUST-1 NFs and PC-HKUST-1 NFs, respectively.

To further evaluate the CH_4 uptake capacities of the different MOF NFs, the CH_4 adsorption isotherms were measured under high pressure. Since this work mainly focused on structuring MOFs for the practical application in ANG system, the CH_4 uptake at around RT was tested, considering CH_4 storage at very low temperature would lead to high operation cost of the ANG system. As shown in Fig. 6a–c, a change of the storage temperature from 313 to 298 K leads to a significant enhancement of the CH_4 volumetric uptake for all the tested MOF NFs. This is consistent with previously reported work [6]. The CH_4 adsorption isotherms were fitted to the multi-site Langmuir model [37], and the corresponding parameters of the fitting are listed in Table S1. However, the CH_4 volumetric uptakes of the three types of HKUST-1 NFs at 3500 kPa are remarkably different, with the following order: DE-HKUST-1 NFs (15 $cm^3 g^{-1}$) < IG-HKUST-1 NFs (40 $cm^3 g^{-1}$) < PC-HKUST-1 NFs (86 $cm^3 g^{-1}$) (Fig. 6d). The lowest CH_4 volumetric uptake for the DE-HKUST-1 NFs demonstrates the severe blockage of MOF pores by the PAN, thus leading to the loss of space/sites for adsorbing CH_4. For IG-HKUST-1 NFs, the *in-situ* growth of MOF crystals on the surface of PAN NFs could avoid the blockage problem. However, the low loading of HKUST-1 in IG-HKUST-1 NFs limits further improvement of the total CH_4 uptake capacity. Among all NF samples, PC-HKUST-1 NFs offer the highest CH_4 uptake capacity, thanks to an exceptionally high loading with

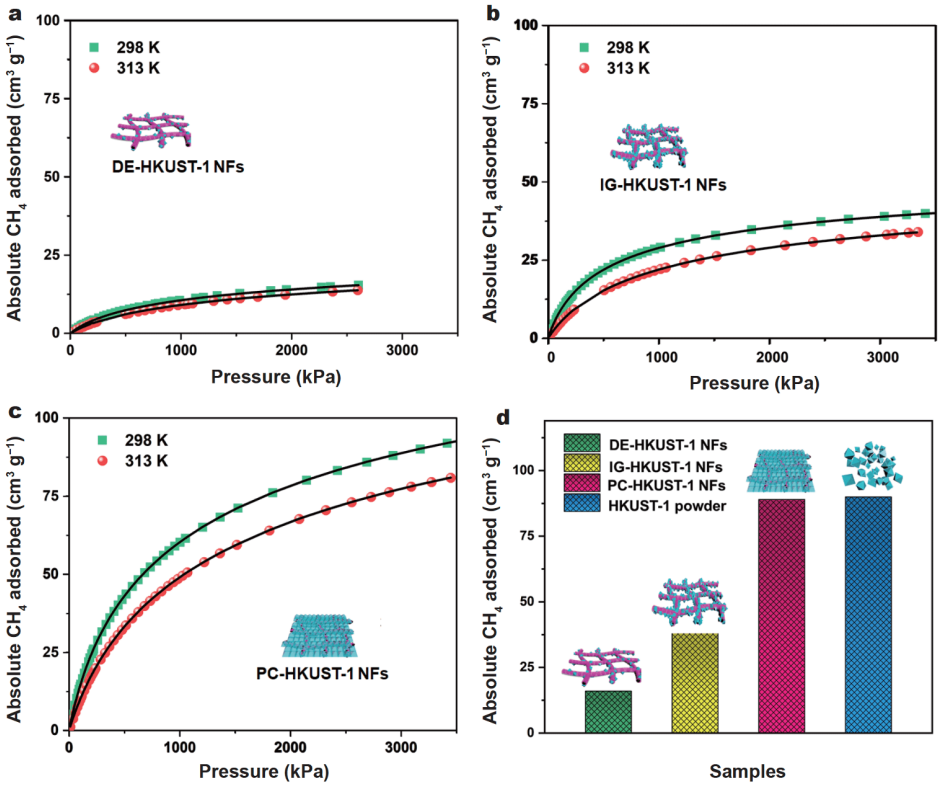

Figure 6 CH_4 isothermal adsorption and multi-site Langmuir fitting curves for the different MOF NF composites: (a) DE-HKUST-1 NFs, (b) IG-HKUST-1 NFs, and (c) PC-HKUST-1 NFs at 298 and 313 K, respectively. (d) The comparison of CH_4 uptake capacity for various NFs: DE-HKUST-1 NFs, IG-HKUST-1 NFs, PC-HKUST-1 NFs, as well as HKUST-1 powder at 3500 kPa and 298 K.

HKUST-1 crystals (~52 wt%), which are fully accessible to CH_4 gas molecules. It should be noted that the CH_4 uptake capacity for the PC-HKUST-1 NFs is even comparable to that of the unstructured HKUST-1 powder (Fig. S9). However, the CH_4 adsorption of PC-HKUST-1 NFs is still lower than the theoretical CH_4 volumetric uptake of 124 $cm^3\ g^{-1}$. Relative large losses in adsorption capacities are currently one of the main challenges for MOF applications in the industry [38]. Here, we attributed the observed reduction in adsorption capacity to the shaping process for MOFs into NFs, as compared with non-structured MOF nanoparticles. To understand the high CH_4 adsorption capacity achieved by the phase conversion method, we carried out the synthesis of HKUST-1 powder by converting $Cu(OH)_2$ to HKUST-1 without PAN NF scaffold. The resulting HKUST-1 powder shows a BET surface area of ~1780 $m^2\ g^{-1}$ (Fig. S10). This represents an increase of ~50% as compared with the surface area of ~1190 $m^2\ g^{-1}$ for HKUST-1 by the conventional synthesis method (Fig. S7). Nevertheless, the CH_4 storage capacity on PC-HKUST-1 NFs was still lower than the recently reported MOFs such as UTSA-76, MOF-519, NU-111, MOF-905, soc MOF and Co(bdp) [39–46]. The reason is that the structuring process led to the loss of CH_4 uptake. Thus, the follow-up work for us is to focus on further process optimization for the structuring of the porous material to improve the CH_4 storage capacity. Furthermore, the heat of adsorption for CH_4 for the three different HKUST-1 NFs was also investigated. The Clausius-Clapeyron equation was used to estimate the heat of adsorption based on the isotherms (Fig. S11). The heat of adsorption of the multi-site Langmuir model (Table S1) corresponds to the heat of adsorption at zero loading. It should be noted that the PC-HKUST-1 NFs exhibit stable CH_4 uptake capacity during the cyclic adsorption test, which is attributed to the high structural stability of PC-HKUST-1 NF mat. As shown in Fig. S12, the morphology and structure of PC-HKUST-1 NFs remain unchanged after the mat was folded for compaction in the container and used for gas adsorption tests. Thus, the novel phase conversion method enables us to structure HKUST-1 nanoparticles into a 3D NF mat with high loading and highly stable CH_4 adsorption performance.

CONCLUSIONS

In summary, we developed a phase conversion method to effectively load MOFs in the large pore space of PAN NFs. At the highest MOF loading of ~52 wt%, the PC-HKUST-1 NFs demonstrated a remarkable enhancement in CH_4 storage capacity compared with DE and IG methods. The high gas adsorption capacity of PC-HKUST-1 NFs can be attributed to the combination of the high surface area of the HKUST-1 crystals that were synthesized by the phase conversion method and the high accessibility of gas molecules to the adsorption sites of the MOF crystals that were grown at the surface and in the pores of the PAN polymer NFs. Furthermore, the method of preparing MOF NFs by phase conversion, which was investigated here for CH_4 adsorption, is also a very promising method for fabricating MOF NFs for a wide range of energy and environmental applications.

Received 12 August 2020; accepted 25 November 2020; published online 10 February 2021

1 Cherp A, Jewell J, Vinichenko V, *et al.* Global energy security under different climate policies, GDP growth rates and fossil resource availabilities. Climatic Change, 2016, 136: 83–94
2 Montoya JH, Seitz LC, Chakthranont P, *et al.* Materials for solar fuels and chemicals. Nat Mater, 2016, 16: 70–81
3 Li XB, Tung CH, Wu LZ. Semiconducting quantum dots for artificial photosynthesis. Nat Rev Chem, 2018, 2: 160–173
4 Makal TA, Li JR, Lu W, *et al.* Methane storage in advanced porous materials. Chem Soc Rev, 2012, 41: 7761–7779
5 Lee S, Kim B, Kim J. Predicting performance limits of methane gas storage in zeolites with an artificial neural network. J Mater Chem A, 2019, 7: 2709–2716
6 Lin RB, He Y, Li P, *et al.* Multifunctional porous hydrogen-bonded organic framework materials. Chem Soc Rev, 2019, 48: 1362–1389
7 Lozano-Castelló D, Alcañiz-Monge J, de la Casa-Lillo MA, *et al.* Advances in the study of methane storage in porous carbonaceous materials. Fuel, 2002, 81: 1777–1803
8 Santos JC, Lima JA, Gurgel JM, *et al.* Improvement of methane storage capacity in activated carbon bed with bidisperse packing. Braz J Chem Eng, 2016, 36: 831–843
9 Kang Z, Xue M, Fan L, *et al.* Highly selective sieving of small gas molecules by using an ultra-microporous metal-organic framework membrane. Energy Environ Sci, 2014, 7: 4053–4060
10 Eddaoudi M, Kim J, Rosi N, *et al.* Systematic design of pore size and functionality in isoreticular MOFs and their application in methane storage. Science, 2002, 295: 469–472
11 Bourrelly S, Llewellyn PL, Serre C, *et al.* Different adsorption behaviors of methane and carbon dioxide in the isotypic nanoporous metal terephthalates MIL-53 and MIL-47. J Am Chem Soc, 2005, 127: 13519–13521
12 Gedrich K, Senkovska I, Klein N, *et al.* A highly porous metal-organic framework with open nickel sites. Angew Chem Int Ed, 2010, 49: 8489–8492
13 Zhao XL, Sun D, Yuan S, *et al.* Comparison of the effect of functional groups on gas-uptake capacities by fixing the volumes of cages A and B and modifying the inner wall of cage C in *rht*-type MOFs. Inorg Chem, 2012, 51: 10350–10355
14 Tanaka S, Sakamoto K, Inada H, *et al.* Vapor-phase synthesis of ZIF-8 MOF thick film by conversion of ZnO nanorod array. Langmuir, 2018, 34: 7028–7033
15 Yang P, Mao F, Li Y, *et al.* Hierarchical porous Zr-based MOFs synthesized by a facile monocarboxylic acid etching strategy. Chem Eur J, 2018, 24: 2962–2970
16 Wang B, Zhao M, Li L, *et al.* Ultra-thin metal-organic framework nanoribbons. Natl Sci Rev, 2020, 7: 46–52
17 Shu Y, Hao JN, Niu D, *et al.* A smart luminescent metal-organic framework-based logic system for simultaneous analysis of copper ions and hydrogen sulfide. J Mater Chem C, 2020, 8: 8635–8642
18 Majano G, Pérez-Ramírez J. Scalable room-temperature conversion of copper(II) hydroxide into HKUST-1 ($Cu_3(btc)_2$). Adv Mater, 2013, 25: 1052–1057
19 Bazer-Bachi D, Assié L, Lecocq V, *et al.* Towards industrial use of metal-organic framework: Impact of shaping on the MOF properties. Powder Tech, 2014, 255: 52–59
20 Furukawa S, Reboul J, Diring S, *et al.* Structuring of metal-organic frameworks at the mesoscopic/macroscopic scale. Chem Soc Rev, 2014, 43: 5700–5734
21 Stassen I, Burtch N, Talin A, *et al.* An updated roadmap for the integration of metal-organic frameworks with electronic devices and chemical sensors. Chem Soc Rev, 2017, 46: 3185–3241
22 Li S, Huo F. Metal-organic framework composites: From fundamentals to applications. Nanoscale, 2015, 7: 7482–7501
23 Dou Y, Zhang W, Kaiser A. Electrospinning of metal-organic frameworks for energy and environmental applications. Adv Sci, 2020, 7: 1902590
24 Liang H, Jiao X, Li C, *et al.* Flexible self-supported metal-organic framework mats with exceptionally high porosity for enhanced separation and catalysis. J Mater Chem A, 2018, 6: 334–341
25 Talmoudi H, Khenoussi N, Adolphe D, *et al.* An *in situ* crystal growth of metal organic frameworks-5 on electrospun PVA nanofibers. Autex Res J, 2018, 18: 308–313
26 Lee G, Seo YD, Jang J. ZnO quantum dot-decorated carbon nanofibers derived from electrospun ZIF-8/PVA nanofibers for high-performance energy storage electrodes. Chem Commun, 2017, 53: 11441–11444
27 Laurila E, Thunberg J, Argent SP, *et al.* Enhanced synthesis of metal-organic frameworks on the surface of electrospun cellulose nanofibers. Adv Eng Mater, 2015, 17: 1282–1286
28 Zhao J, Lee DT, Yaga RW, *et al.* Ultra-fast degradation of chemical warfare agents using MOF-nanofiber kebabs. Angew Chem Int Ed, 2016, 55: 13224–13228
29 Liu C, Wu YN, Morlay C, *et al.* General deposition of metal-organic frameworks on highly adaptive organic-inorganic hybrid electrospun fibrous substrates. ACS Appl Mater Interfaces, 2016, 8: 2552–2561
30 Ji D, Peng S, Fan L, *et al.* Thin MoS_2 nanosheets grafted MOFs-derived porous Co–N–C flakes grown on electrospun carbon nanofibers as self-supported bifunctional catalysts for overall water splitting. J Mater Chem A, 2017, 5: 23898–23908
31 Zhang Y, Yuan S, Feng X, *et al.* Preparation of nanofibrous metal-organic framework filters for efficient air pollution control. J Am Chem Soc, 2016, 138: 5785–5788
32 Su Z, Zhang M, Lu Z, *et al.* Functionalization of cellulose fiber by *in situ* growth of zeolitic imidazolate framework-8 (ZIF-8) nanocrystals for preparing a cellulose-based air filter with gas adsorp-

tion ability. Cellulose, 2018, 25: 1997–2008
33 Bian Y, Wang R, Wang S, *et al.* Metal-organic framework-based nanofiber filters for effective indoor air quality control. J Mater Chem A, 2018, 6: 15807–15814
34 Fan L, Xue M, Kang Z, *et al.* Electrospinning technology applied in zeolitic imidazolate framework membrane synthesis. J Mater Chem, 2012, 22: 25272–25276
35 Zhang R, Hu L, Bao S, *et al.* Surface polarization enhancement: High catalytic performance of Cu/CuO_x/C nanocomposites derived from Cu-BTC for CO oxidation. J Mater Chem A, 2016, 4: 8412–8420
36 Weng Y, Guan S, Wang L, *et al.* Defective porous carbon polyhedra decorated with copper nanoparticles for enhanced NIR-driven photothermal cancer therapy. Small, 2020, 16: 1905184
37 Grande CA, Blom R, Möller A, *et al.* High-pressure separation of CH_4/CO_2 using activated carbon. Chem Eng Sci, 2013, 89: 10–20
38 Tian T, Zeng Z, Vulpe D, *et al.* A sol-gel monolithic metal-organic framework with enhanced methane uptake. Nat Mater, 2018, 17: 174–179
39 Wilmer CE, Farha OK, Yildirim T, *et al.* Gram-scale, high-yield synthesis of a robust metal-organic framework for storing methane and other gases. Energy Environ Sci, 2013, 6: 1158–1163
40 Gándara F, Furukawa H, Lee S, *et al.* High methane storage capacity in aluminum metal-organic frameworks. J Am Chem Soc, 2014, 136: 5271–5274
41 Jiang J, Furukawa H, Zhang YB, *et al.* High methane storage working capacity in metal-organic frameworks with acrylate links. J Am Chem Soc, 2016, 138: 10244–10251
42 Peng Y, Srinivas G, Wilmer CE, *et al.* Simultaneously high gravimetric and volumetric methane uptake characteristics of the metal-organic framework NU-111. Chem Commun, 2013, 49: 2992–2994
43 Li B, Wen HM, Wang H, *et al.* A porous metal-organic framework with dynamic pyrimidine groups exhibiting record high methane storage working capacity. J Am Chem Soc, 2014, 136: 6207–6210
44 Mason JA, Oktawiec J, Taylor MK, *et al.* Methane storage in flexible metal-organic frameworks with intrinsic thermal management. Nature, 2015, 527: 357–361
45 Alezi D, Belmabkhout Y, Suyetin M, *et al.* MOF crystal chemistry paving the way to gas storage needs: Aluminum-based **soc**-MOF for CH_4, O_2, and CO_2 storage. J Am Chem Soc, 2015, 137: 13308–13318
46 Guo Z, Wu H, Srinivas G, *et al.* A metal-organic framework with optimized open metal sites and pore spaces for high methane storage at room temperature. Angew Chem Int Ed, 2011, 50: 3178–3181

Acknowledgements This work was supported by the Grande Solution Project "HiGradeGas" (48279), and Innovation Fund Denmark, exploring NFs-based adsorbents for biogas upgrading and storage. We also thank the Danish Research Council to provide funding to support fundamental research on electrospinning (8022-00237B) and for investigating NFs structures for enzyme immobilization (6111-00232B).

Author contributions Dou Y, Zhang W, and Kaiser A conceived the idea and prepared the manuscript; Dou Y worked on the synthesis and characterization of MOF NFs; Grande C took part in the CH_4 adsorption measurement. This article was discussed with contributions from all authors.

Conflict of interest The authors declare that they have no conflict of interest.

Supplementary information Supporting data are available in the online version of the paper.

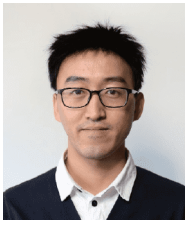

Yibo Dou obtained his BSc and PhD degrees from Beijing University of Chemical Technology in 2009 and 2015, under the supervision of Prof. Xue Duan. Currently, he is a Researcher at the Technical University of Denmark. His main research topic is electrospinning of porous material-based functional nanofibers for energy and environmental applications.

Andreas Kaiser received his PhD degree in chemistry/materials science in 1994 at the University of Würzburg/Fraunhofer Institute for Silicate Chemistry. He is currently an Associate Professor at the Technical University of Denmark. His research interests are on the development of advanced porous materials for energy and environmental applications, including membranes, gas adsorption devices, electrocatalysis and fuel cells/electrolyzers.

Wenjing Zhang received her Master and PhD degrees at the Hong Kong University of Science and Technology. She is currently an Associate Professor and group leader at the Technical University of Denmark, focusing on advanced material design for water treatment, catalysis, fuel cells, water splitting and CO_2 reduction. She is also an Honorary Distinguished Professor at Qingdao University of Science and Technology in China.

多级结构MOFs纳米纤维用于甲烷存储研究

豆义波[1,2], Carlos Grande[3], Andreas Kaiser[1*], 张文静[2*]

摘要 多孔金属有机骨架材料MOFs在气体存储领域具有潜在应用前景，但是其面向实际应用的加工成型仍具有挑战. 本文报道了一种基于静电纺丝技术和相转变结合的方法来构筑MOFs纤维，有效实现了Cu-MOF(HKUST-1)在PAN纳米纤维表面的高效负载. 该方法首先将$Cu(OH)_2$生长在PAN纳米纤维表面，进一步通过相转变获得HKUST-1. 相比之前的文献报道，该HKUST-1纳米纤维表现出更优异的甲烷存储性能，其在3500 kPa和298 K条件下的甲烷存储量达到86 $cm^3\ g^{-1}$. 研究表明该纤维使得负载在表面的MOF高度暴露，具有高的比表面和负载量. 该工作为MOFs加工成型并用于能源和环境领域提供了新的思路.

